Sea Ice Thickness Measurement Using Spaceborne GNSS-R: First Results With TechDemoSat-1 Data

Qingyun Yan, *Student Member, IEEE*, and Weimin Huang, *Senior Member, IEEE*

***Abstract*—In this article, an effective schematic is developed for estimating sea ice thickness (SIT) from the reflectivity (Γ) produced with TechDemoSat-1 (TDS-1) Global Navigation Satellite System-Reflectometry data. Here, Γ is formulated as the product of the propagation loss due to SIT and the reflection coefficient of underlying seawater. The effect of surface roughness on Γ is neglected when only considering signals of coherent reflection. In practice, Γ at the specular point is first generated using TDS-1 data. Afterwards, SIT is calculated from TDS-1 Γ based on the proposed reflectivity model, and verified with two sets of reference SIT data; one is obtained by the Soil Moisture Ocean Salinity (SMOS) satellite, and the other is the combined SMOS/Soil Moisture Active Passive (SMAP) measurements. This analysis is performed on the data with SIT less than 1 m. Through comparison, good consistency between the derived TDS-1 SIT and the reference SIT is obtained, with a correlation coefficient (r) of 0.84 and a root-mean-square difference (RMSD) of 9.39 cm with SMOS, and an r of 0.67 and an RMSD of 9.49 cm with SMOS/SMAP, which demonstrates the applicability of the developed model and the utility of TDS-1 data for SIT estimation. In addition, this method is proved to be useful for improving existing sea ice detection accuracy.**

***Index Terms*—Global navigation satellite system-reflectometry (GNSS-R), sea ice thickness (SIT), soil moisture ocean salinity (SMOS), soil moisture active passive (SMAP), TechDemoSat-1 (TDS-1).**

I. Introduction

A GOOD knowledge of sea ice parameters helps improve the understanding of global climate change and facilitates human activities in ice-covered regions. Recently, sea ice remote sensing has been a topic of interest in Global Navigation Satellite System-Reflectometry (GNSS-R) circles due to public access to the data provided by the TechDemoSat-1 (TDS-1) satellite. Significant progress has been made in sea ice detection [1]–[5], type classification [6], sea ice concentration (SIC) estimation [7], [8], ice sheet [9], [10], and sea ice [11], [12] altimetry. Furthermore, a comprehensive review of sea ice sensing using GNSS-R has been presented in [13]. Nonetheless, limited work has been done for obtaining sea ice thickness (SIT), which is another important sea ice parameter. A preliminary experiment in [12] found that the main reflection was from the ice-seawater interface and showed the potential of TDS-1 GNSS-R signals for estimating SIT, based on the fact that the difference between the retrieved surface elevation and the mean sea surface is highly correlated with collocated SIT (with a correlation coefficient of 0.71). However, that method relies on an ad hoc orbit discrepancy correction and employs limited satellite raw data, which reduces its general applicability. The achieved altimetric accuracy with a root-mean-square difference (RMSD) of 4.7 cm compared with the mean sea surface should be highlighted.

At present, large-scale SIT data can be derived from 1) sea ice elevation (freeboard) measurement by satellite altimeters, e.g., European Remote Sensing [14], ENVISAT [15], and CryoSat-2 [16], based on the conversion between SIT and freeboard; or 2) microwave radiometry, e.g., Soil Moisture Ocean Salinity (SMOS) [17] and Soil Moisture Active Passive (SMAP) [18], according to the model of brightness temperature measurement and SIT [19]. For GNSS-R, the altimetry technique can be applied for SIT estimates, but the error obtained is severe with an RMSD of 4.4 m [11], which will lead to a high discrepancy in SIT estimation. In addition, Mayers and Ruf [20] confirmed the possibility of measuring SIT with GNSS-R based on simulated data. This method, however, cannot be implemented currently due to lack of raw data. Therefore, a new scheme for estimating SIT needs to be devised for GNSS-R. As such, in this article, a model is developed for retrieving SIT from a TDS-1 reflectivity (Γ). The SIT estimates are validated with two different reference data: 1) the SMOS results from the University of Hamburg, and 2) the combined SMOS/SMAP measurements from the University of Bremen, with good consistency. The remainder of the article is organized as follows. Section II introduces the experimental and reference data. The proposed Γ-based SIT estimation scheme is described in Section III. Results and discussions are presented in Section IV, followed by conclusion in Section V.

II. Data Description

A. TDS-1 Remote Sensing Data

In this article, the remote sensing data used for SIT retrieval are from the TDS-1 satellite, which provides a good coverage over northern high-latitude ice-covered regions in seas above 80°. The dataset used in this work spans over a period from December 2016 to December 2018. The data employed for deriving Γ at specular point (SP) include the following:

Manuscript received August 7, 2019; revised December 5, 2019 and December 29, 2019; accepted January 12, 2020. Date of publication January 22, 2020; date of current version February 13, 2020. This work was supported by the Canada First Research Excellence Fund, through the Ocean Frontier Institute. The work of W. Huang was supported in part by the Natural Sciences and Engineering Research Council of Canada Discovery under Grant NSERC RGPIN-2017-04508 and Grant RGPAS-2017-507962 and in part by the Canadian Space Agency CubeSat under Grant 17CCPNFL11. *(Corresponding author: Weimin Huang.)*

The authors are with the Faculty of Engineering and Applied Science, Memorial University, St. John's, NL A1B 3X5, Canada (e-mail: qy2543@mun.ca; weimin@mun.ca).

Digital Object Identifier 10.1109/JSTARS.2020.2966880

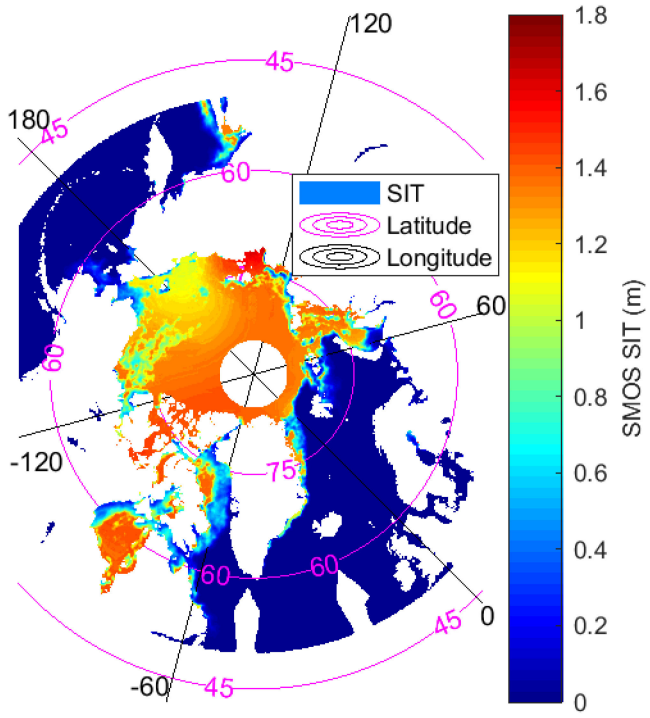

Fig. 1. Example of reference SMOS SIT data for February 3, 2018. Regions without data are colored in white.

1) the delay-Doppler map (DDM) files (depicting scattering power over surfaces);
2) the metadata files (providing locations of the transmitter and receiver, the incidence angle, the antenna gain, and the acquisition time);
3) the direct signal power files (measuring the direct signal power from transmitter).

The total amount of data for TDS-1 measurements examined in this article is more than 4.8 million samples, which were collected from 42714 tracks, separately.

B. Reference Data

1) Γ Reference–Cyclone GNSS (CYGNSS): CYGNSS was launched in 2016, and has provided measurements since March 2017. It only covers low-latitude regions between 40°S and 40°N, thus, it is of limited application for sea ice sensing. However, it allows reflectivity estimation, which is employed, here, to validate the derived TDS-1 Γ for subsequent SIT estimation. Data with a signal-to-noise ratio (SNR) over 3 dB at SP and with an incidence angle less than 30° at SP are retained here.

2) SIT Reference–SMOS and Combined SMOS/SMAP: Annually, since 2010, SMOS [17] has produced daily SIT data in the northern hemisphere during intervals from October 15 to April 15. An example of SMOS SIT data is shown in Fig. 1. The uncertainty in such SIT data is available and necessary for quality control purposes. In this article, SIT data with uncertainties over 0.5 m are discarded. As a result, the maximum SIT of selected reference data is about 0.8 m. Because of the low uncertainty with data, the SMOS SIT is regarded as ground truth in this article. In addition, the dataset also includes sea ice salinity and temperature information, which will be treated as *a priori* information here. Since these two parameters can be dependent on the associated SIT, another SIT product that combines SMOS and SMAP measurements [18] was also employed for validation.

III. Retrieval of SIT From Reflectivity

A. Derivation of Reflectivity

It has been demonstrated that the GNSS-R signal received over sea ice is usually a coherent reflection due to its smooth surface [1], [2]. For coherent reflection, Γ at SP can be obtained with the corresponding received power through [21], [22]

$$\Gamma = \frac{16\pi^2}{\lambda^2}\frac{P_r}{P_t}\frac{(R_t + R_r)^2}{G_t G_r} \tag{1}$$

where $\lambda = 19$ cm is the GNSS-R signal wavelength, and P_t and P_r denote the transmitted and received power, respectively. G_t and G_r represent the antenna gains of the transmitter and receiver, and R_t and R_r are the distances from the transmitter and receiver to the specular point.

G_r at SP can be obtained from the metadata file. R_t and R_r can be easily derived given the positions of the transmitter, receiver, and SP, which are also provided in the metadata. For each DDM, the column with zero-Doppler shift (also known as the delay waveform) is extracted. The average of the first four bins in the delay waveform is regarded as the noise floor and subtracted from the delay waveform. Next, P_r at SP is determined as the power value of the bin with the maximum first-order derivative of the waveform, as described in [23]. The availability of direct signal power files (that record the direct signal from the transmitter at zenith) improves the estimate of the transmitted signal power, which can be derived through

$$P_t G_t = 4\pi R_d^2 G_d P_d \tag{2}$$

where R_d is the distance from transmitter to receiver, P_d is the direct power, and G_d is the zenith antenna gain. Lacking precise knowledge of G_d, it is set as 3 in this article, using the gain at 90° provided by [24].

As P_r is taken from a region immediately surrounding the SP, the value of Γ and above-mentioned parameters are assumed to be constant over this region [25]. In the case of coherent reflection, the area of this region can be determined as the size of the first Fresnel zone, which is about several hundred meters depending on the geometry [26], and it is regarded as the spatial resolution of this method.

B. Relationship Between SIT and Γ

For coherent reflection, Γ can be modeled as [27]

$$\Gamma = |R|^2 \cdot \exp\left[-\left(\frac{4\pi}{\lambda}\sigma_{\text{rms}}\cos\theta\right)^2\right] \tag{3}$$

where R is the Fresnel reflection coefficient, σ_{rms} is the surface RMS height, and θ is the incidence angle. The second term in this equation depicts the roughness; it is clear that this term is approximately 1 for smooth surfaces with a very small σ_{rms}, and

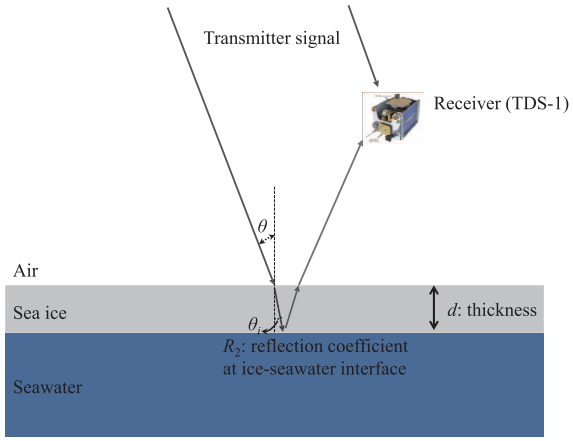

Fig. 2. Schematic of GNSS-R signal reflected from a three-layer model of air, sea ice, and seawater.

thus, the following approximation can be made:

$$\Gamma = |R|^2. \tag{4}$$

Henceforth, only the TDS-1 measurement of coherent reflection will be considered for SIT retrieval based on (4).

Considering a three-layer air-ice-seawater model (see Fig. 2 for illustration), R can be expressed as [28]

$$R = \frac{R_1 + R_2 e^{-2ik_{zi}d}}{1 + R_1 R_2 e^{-2ik_{zi}d}} \tag{5}$$

where R_1 and R_2 denote the reflection coefficients at the upper (air-sea ice) and lower (sea ice–seawater) interfaces, respectively, d is SIT, and k_{zi} is the z-component of the signal propagation vector in the sea ice. The formula of k_{zi} contains a real part, which is referred to as the phase constant β, and an imaginary part, which is called the attenuation coefficient α, and is given as

$$k_{zi} = \beta - i\alpha. \tag{6}$$

As pointed out in [12], due to a lower dielectric difference between air and sea ice than that between sea ice and seawater, R_1 is less than R_2, and accordingly, the signals are mainly reflected by the ice-water interface for the case of first-year sea ice with a thickness of 20 to 60 cm. This is supported by the finding in [12] that the gap between the estimated surface elevation and the mean sea surface is highly correlated with local SIT. A similar phenomenon of strong reflection from the ice-water layer is also noted in [29] and [30]. For this reason, the factor of R_1 in (5) can be neglected by being set as 0 here, which gives

$$R \approx R_2 e^{-2ik_{zi}d} \tag{7}$$

and by combining (4), (6), and (7), we have

$$\Gamma = |R_2|^2 e^{-4\alpha d}. \tag{8}$$

The expression for α is (see e.g., [19])

$$\alpha = \frac{2\pi}{\lambda} \cos\theta \left|\mathrm{Im}\left\{\sqrt{\varepsilon_i}\right\}\right| \tag{9}$$

with ε_i being the relative permittivity of sea ice.

In summary, in this article the reflectivity Γ of an ice-covered sea surface is modeled as the product of the propagation loss within the ice layer and the reflection coefficient at the ice-seawater interface. In the proposed model, signals are first attenuated by the ice layer and then reflected at the ice-water interface. Thus, SIT d can be estimated as

$$d = \frac{-1}{4\alpha} \ln \frac{\Gamma}{|R_2|^2} \tag{10}$$

with Γ and the values of R_2 and α, whose derivation will be described in the following section.

C. Dielectric Models

From (9), it can be seen that α is dependent on ε_i. The model of [31] is adopted, here, for obtaining ε_i based on the relative brine volume (V_b, in ‰, or per thousand)

$$\varepsilon_i = 3.1 + 0.0084 V_b + i(a_1 + a_2 V_b) \tag{11}$$

with $a_1 = 0.037, a_2 = 0.00445$ for first-year ice, or $a_1 = 0.003, a_2 = 0.00435$ for multiyear ice. To derive V_b, the following empirical formula, which was presented in [32] can be used

$$V_b = 10^{-3} S \left(-\frac{49.185}{T} + 0.532\right) \tag{12}$$

where S and T are sea ice salinity (in ‰) and temperature (in degrees Celsius), respectively.

R_2 can be expressed by the combination of horizontally and vertically polarized reflection coefficients (i.e., R_{hh} and R_{vv}) [33], as

$$R_2 = \frac{1}{2}(R_{vv} - R_{hh}) \tag{13}$$

and

$$R_{vv} = \frac{\varepsilon_r \cos\theta_i - \sqrt{\varepsilon_r - \sin^2\theta_i}}{\varepsilon_r \cos\theta_i + \sqrt{\varepsilon_r - \sin^2\theta_i}} \tag{14}$$

$$R_{hh} = \frac{\cos\theta_i - \sqrt{\varepsilon_r - \sin^2\theta_i}}{\cos\theta_i + \sqrt{\varepsilon_r - \sin^2\theta_i}} \tag{15}$$

$$\theta_i = \arcsin \frac{\sin\theta}{\sqrt{\varepsilon_i}} \tag{16}$$

$$\varepsilon_r = \varepsilon_w / \varepsilon_i \tag{17}$$

and θ_i is the incidence angle in the sea ice, and ε_w is the relative permittivity of seawater, which can be calculated using the model of [34].

Therefore, the estimated SIT from the TDS-1 Γ can be obtained based on (10); and (1) and (2) for Γ, (11)–(17) for R_2, and (9), (11), and (12) for α.

IV. Results

A. Data Quality Control

In this article, only DDMs of coherent reflection were employed. This data selection process is based on the pixel number

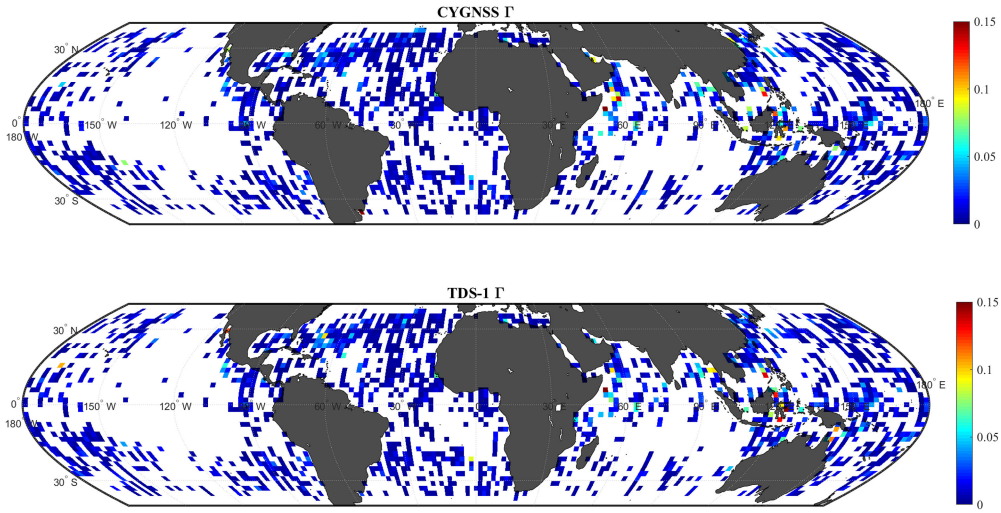

Fig. 3. Comparison between the CYGNSS and TDS-1 Γ. Correlation coefficient of $r = 0.83$ and an RMSD of 0.01 are obtained.

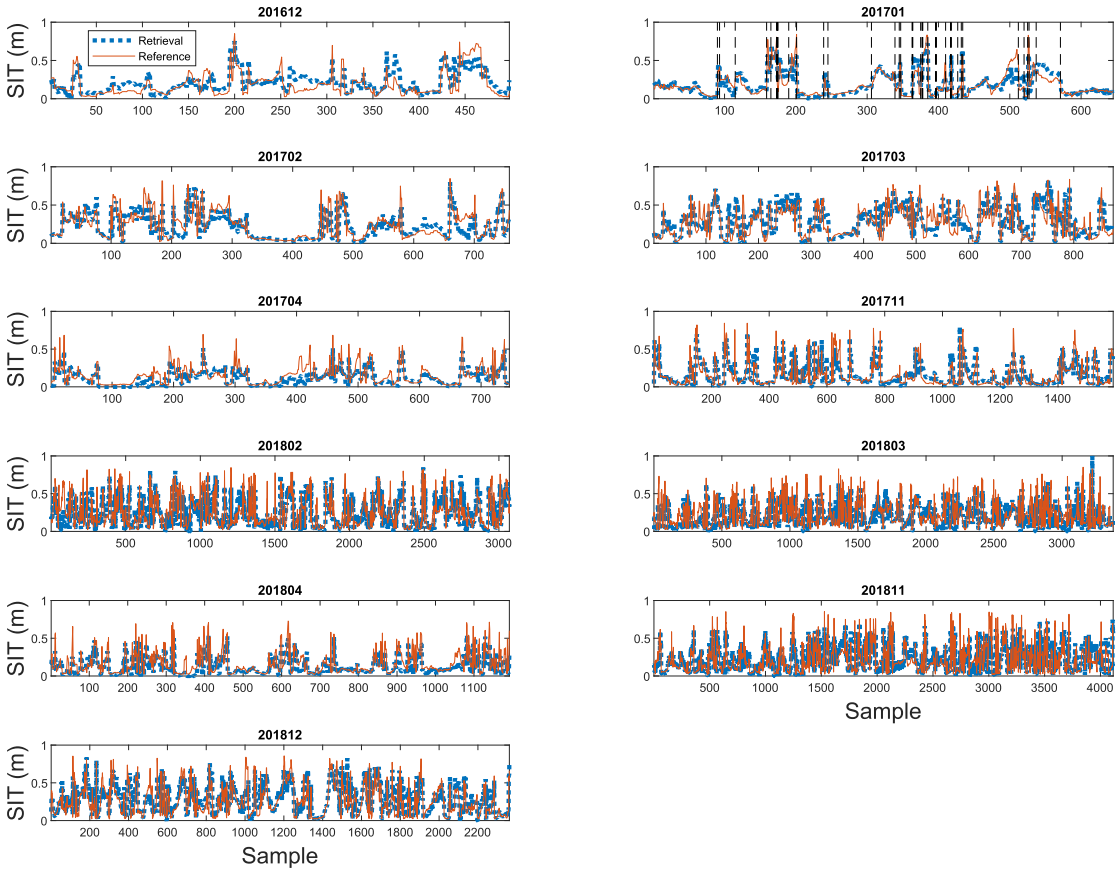

Fig. 4. Comparison of SIT estimation results by month: TDS-1 and SMOS. As an example (January 2017), the results obtained within the same track were grouped together by blocks separated by vertical dashed lines. Although offsets between the two measurements can be observed, the changing trend of the results within each track agrees very well.

observable proposed in [1] (see [1], [2] for other optional approaches). It is worth mentioning that a spreading of the DDM has also been observed in some cases over sea ice, suggesting that the scattering might contain a relevant incoherent component superimposed to the coherent one [2]. However, we attempt to omit such data by discarding them according to the pixel number observable. In addition, following [10], data with high incidence angles were also excluded. In addition, noisy data were rejected according to the SNR at SP. In summary, the TDS-1 dataset used here meets the following specific requirements.

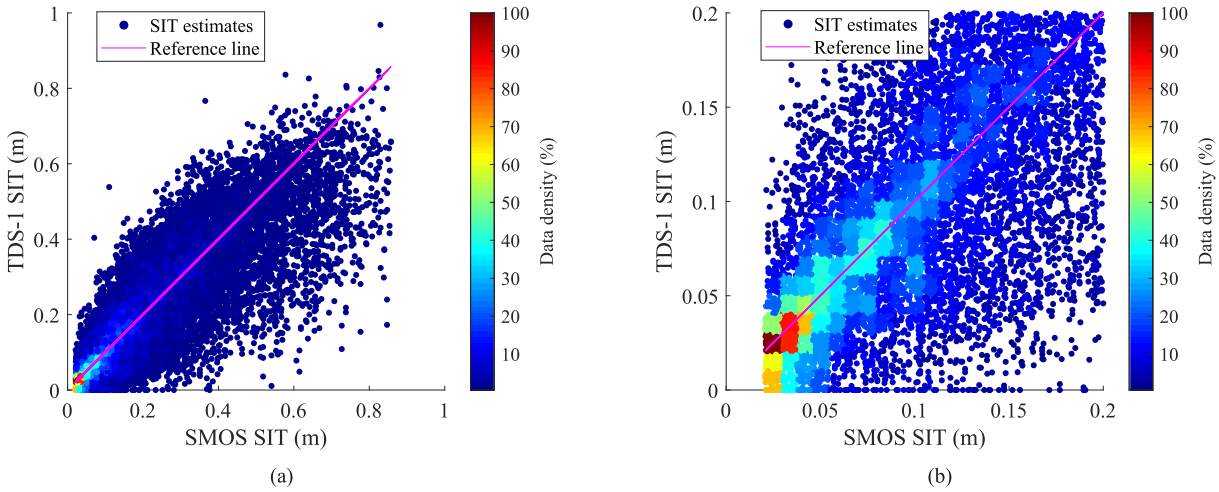

Fig. 5. Density plot comparing SIT from TDS-1 retrieval and collocated SMOS data with the 1:1 reference line (magenta). (a) All results. (b) SMOS SIT below 0.2 m.

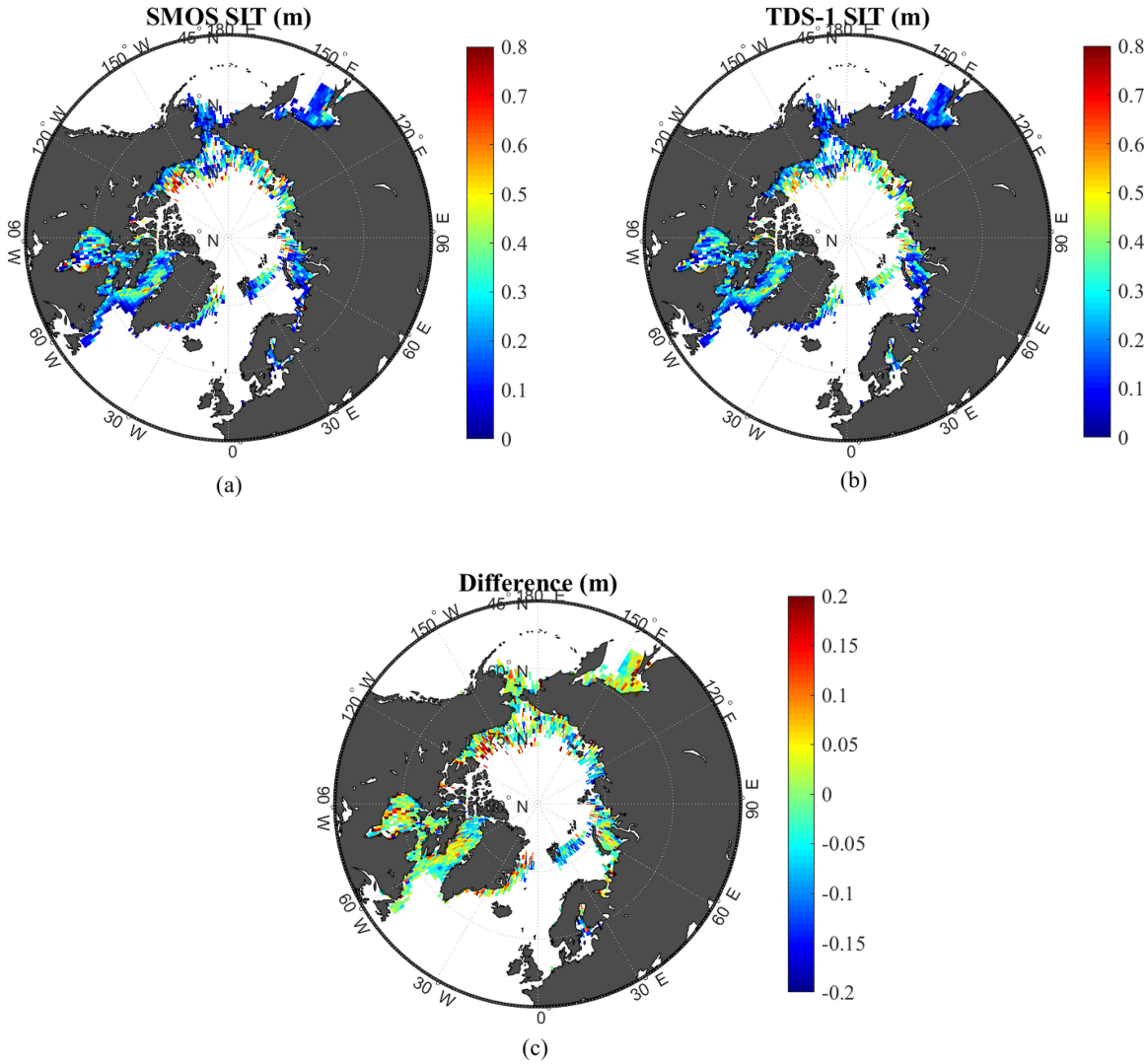

Fig. 6. SIT values. (a) SMOS data. (b) TDS-1 results. (c) Difference between the SMOS and TDS-1 SIT. Regions without data are in white.

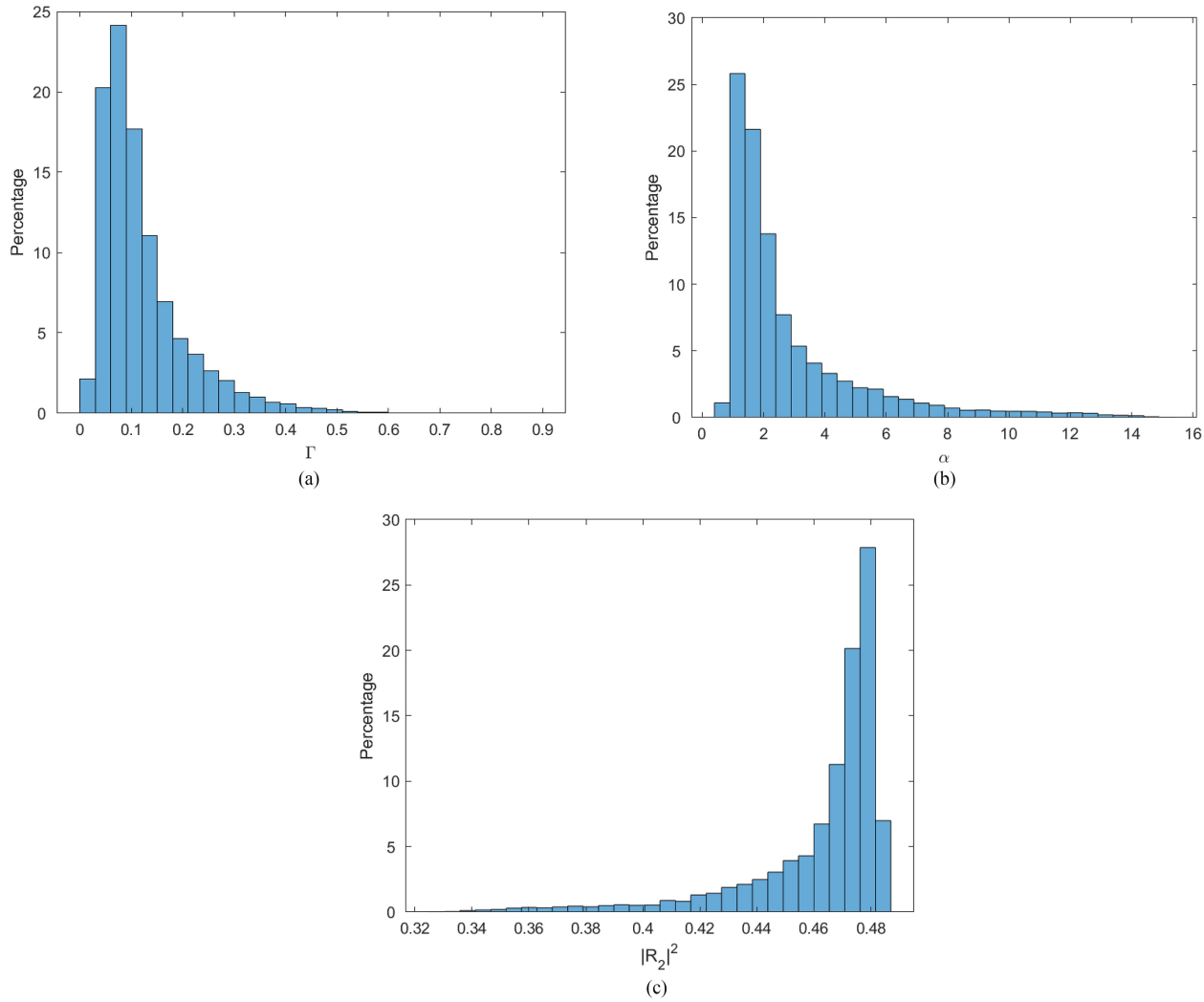

Fig. 7. Histograms of: (a) Γ, (b) α, and (c) $|R_2|^2$.

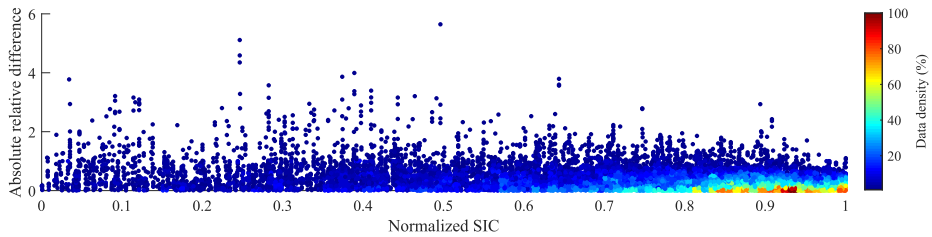

Fig. 8. Impact of SIC on the accuracy of SIT retrieval. Higher SIC generally results in less discrepancy.

1) The incidence angle at SP is less than 30°.
2) The SNR at SP is greater than 3 dB.
3) The number of pixels with over 10% peak power is less than 20.

After applying this data quality control strategy, 18 511 measurements were retained for SIT estimation, and 11 401 for Γ verification. The difference in the amount of the data used for these two applications lies in the spatial and temporal variations.

B. Γ: *CYGNSS and TDS-1*

In this article, Γ was generated from the TDS-1 data. First, the TDS-1 data were calibrated based on gain measurement following the steps described in [35]. The same calibration process was also used by [6]. After calibration, the unit of received power has been changed from counts to watts, and the gain and range variables were used to determine Γ as stated by (1) and (2) in Section III-A.

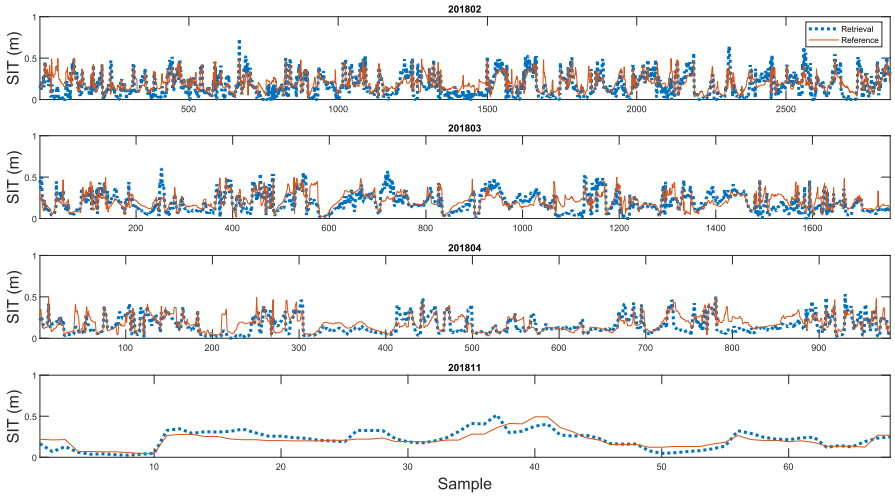

Fig. 9. Monthly comparison of SIT results between TDS-1 and the combined SMOS/SMAP.

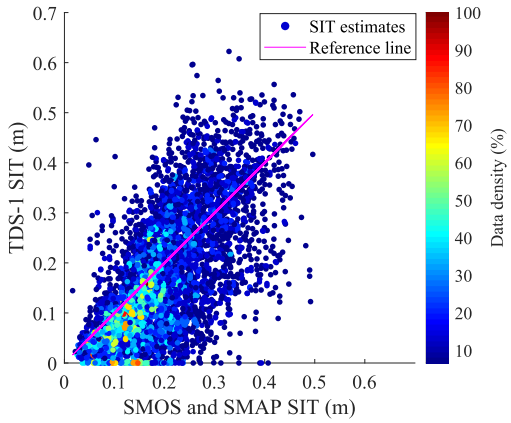

Fig. 10. Density plot comparing SIT from TDS-1 retrieval and collocated combined SMOS/SMAP data with the 1:1 reference line (magenta).

In order to verify the produced TDS-1 Γ result, it was compared with the collocated Γ provided by another available GNSS-R system (i.e., CYGNSS), since these two systems have some overlapping on their operation periods from March 2017 to December 2018. Comparison was made between these two results only over ocean surfaces, with a distance less than 10 km and a time gap of less than 30 min. Despite small temporal and spatial discrepancies, both sets of results agree very well with each other, offering a correlation coefficient (r) of 0.83 and an RMSD of 0.01. These results are plotted in a $2^\circ \times 2^\circ$ (latitude/longitude) grid over the region from 40 °S to 40 °N, as shown in Fig. 3.

C. SIT Estimate: SMOS and TDS-1

This section demonstrates the validation of TDS-1 SIT against the SMOS and SMOS/SMAP references. In order to ensure the quality of the reference data, only those with low uncertainties (less than 0.5 m) were retained. For the data studied, it turned out that the SIT under investigation was generally below 1 m, which fell in the category of first-year ice. Thus, the parameters for first-year ice were applied to (11). The associated SMOS sea ice temperature and salinity data were treated as known in this article, and as such, SIT was estimated based on this proposed method.

The available results were grouped by month and displayed in Fig. 4. Note that monthly data absences were observed in both the TDS-1 and SMOS data, and the amount of qualified TDS-1 data varied among months. Nonetheless, the proposed method still showed its generality and effectiveness over different periods, since no obvious discrepancy was seen in the monthly results. The overall results were plotted in the form of a density plot (see Fig. 5), which indicated a good agreement (specifically, an r of 0.84 and an RMSD of 9.39 cm) between the TDS-1 and SMOS results, especially for the most dense data. The data densities were calculated relative to the maximum of their distribution. Due to the constraint of the SMOS data in spatial coverage, comparison was only performed for the northern hemisphere. Here, the region with a latitude above 45°N was divided into grids of $1^\circ \times 1^\circ$. The overall TDS-1 and SMOS SIT results were separately plotted into these grids based on their latitudes and longitudes, and averaged (see Fig. 6). Over this region, the difference between the averages was found to be trivial. This further validated the robustness of developed method for various regions. Good performance in terms of both spatial and temporal variability suggests the feasibility of the proposed model with TDS-1 data for SIT estimation. The histograms of Γ, α, and $|R_2|^2$ are displayed in Fig. 7.

It is worth mentioning that the GNSS-R measuring geometry and power configurations of different operational tracks can vary significantly. Accordingly, the error level of the Γ retrieval and the subsequent SIT results can change notably. However, it was found, here, that the variation of system configurations within the same track was negligible. Thus, it is meaningful to inspect the changing trends of both TDS-1 and SMOS SITs within each track. Take the results of January 2017 as an example (see Fig. 4), regardless of offset between these two SITs, they generally followed the same tendency within each track (that was divided by vertical lines).

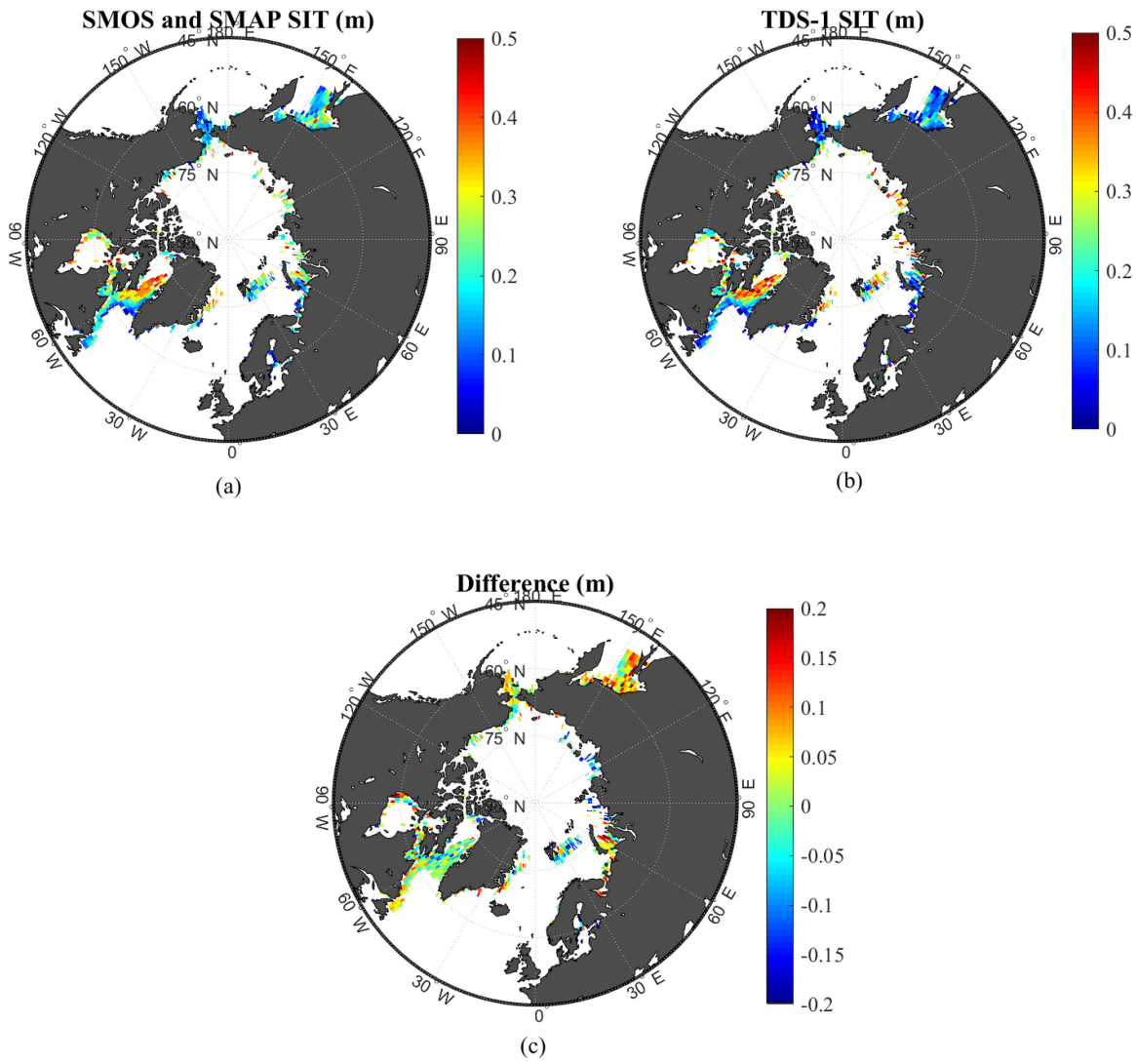

Fig. 11. SIT values. (a) Combined SMOS/SMAP data. (b) TDS-1 results. (c) Difference between the combined SMOS/SMAP and TDS-1 SIT. Regions without data are in white.

It should be pointed out that the retrieved SIT result is also sensitive to sea ice concentration. The absolute value of the relative difference between the retrieved SIT and SMOS reference for varying SICs has been depicted in Fig. 8. It can be found in general that the higher the SIC is, the more accurate the retrieved result will be.

The SMOS SIT data used previously are provided by the University of Hamburg. Their corresponding S and T data were employed for SIT estimation in this article to compare with the SMOS results. It may be better to use the SMOS S and T and compare the SIT estimation result with a different data source. In order to further validate the retrieval results, comparison with the combined SMOS/SMAP data from University of Bremen [18] is also conducted, and the corresponding RMSD and correlation coefficient are 9.49 cm and 0.67, respectively. Similarly, the monthly comparison, density plot, and spatial distribution results are displayed in Figs. 9–11, respectively. Both the mean and standard deviation of the errors (for both reference datasets) as a function of SIT are provided in Fig. 12. In general, these errors increase with higher SITs. In order to check the sensitivity of SIT to Γ, α, and $|R_2|^2$, each of these variables was replaced by its median value for the retrieval and the corresponding variations in RMSD are 1.92, 0.23, and 0.10 cm, respectively. Thus, SIT estimation is found to be most sensitive to variation in Γ.

It should be noted that both GNSS-R and SMOS/SMAS adopt *L*-band signals, and their frequencies, specifically, 1.57 GHz for GNSS-R and 1.41 GHz for SMOS/SMAP, are close to each other. Thus, their sensitivity to SIT with respect to signal frequencies is similar.

D. Case Study

It should be noted that the results associated with the data whose ratio between Γ and $|R_2|^2$ (or equivalently, $e^{-4\alpha d}$) is greater than 1 were assigned a SIT estimate of 0; there are 180 such measurements (out of 18 511) found in the data examined

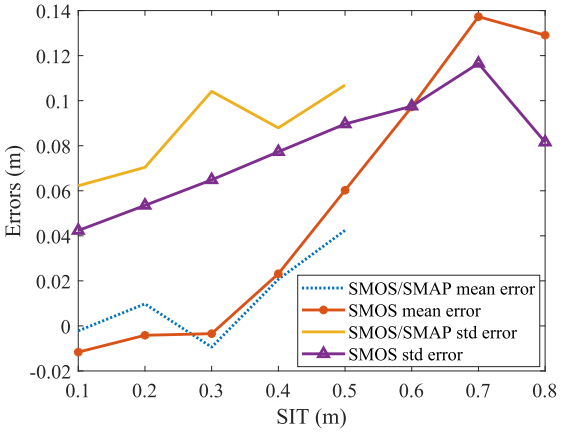

Fig. 12. Mean and standard deviation of the errors using two reference data. Note that the employed SMOS/SMAP SITs are below 0.5 m and SMOS SITs are lower than 0.8 m.

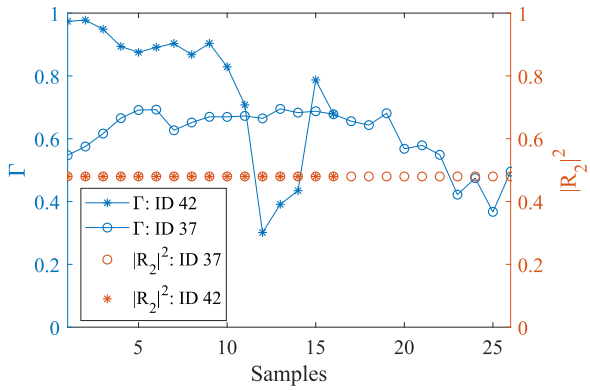

Fig. 14. Values of Γ and $|R_2|^2$ for calm sea conditions. Data are from tracks no. 37 and no. 42 that were measured on 14 April, 2018.

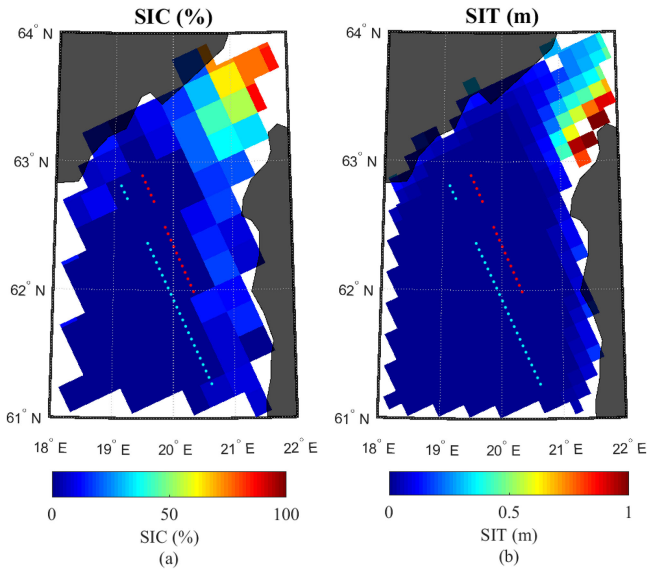

Fig. 13. Collocated reference. (a) SIT. (b) SIC data, confirming the absence of sea ice during the TDS-1 measurement over tracks of no. 37 (cyan dots) and no. 42 (red dots).

in this article. A ratio greater than 1 indicates there was no attenuation caused by the sea-ice. This offers a new perspective of the proposed scheme for improving existing sea ice detection methods, in which false alarms may be made for the cases of coherent reflection from calm ocean surfaces [1], [36], and the power strength was not taken into account. Here, the following cases are studied as a proof of concept.

The specific region under investigation is illustrated in Fig. 13, and the date is 14 April, 2018. TDS-1 measurements from two different tracks (no. 37 that is in cyan dots and no. 42 in red) were employed. The absence of sea ice was further confirmed based on the SIC reference data (from [37]) of 0 over these tracks. Moreover, the sea state was found to be low, with a wind speed of about 4 m/s during this period, according to the ERA-Interim data [38]. In the ice-free scenario, $|R_2|^2$ was calculated by setting ε_i as 1 (the relative permittivity of air). In general, the derived Γ is higher than $|R_2|^2$ (see Fig. 14), which demonstrated the absence of sea ice. However, by using existing sea ice detection methods (in which the value of signal power at SP was ignored), these measurements would produce false alarms of sea ice.

E. Error Source Analysis

This section lists several sources that can be responsible for the difference between the TDS-1 and SMOS SITs. These include the reference data uncertainty, the error introduced by using a simplified model, and drawbacks of TDS-1 in measuring Γ.

First, the uncertainty of the SMOS SIT data employed can be up to 0.5 m. In addition, the SMOS sea-ice temperature and salinity data are used as inputs, whose accuracy is also critical for the SIT estimation. It is found that R_2 ranges from 0.57 to 0.70 based on all the T and S values considered. Taking this result as the maximum uncertainty, the maximum bias of SIT estimation is only 0.04 m.

Second, it should be noted that (7) was developed from ignoring R_1 in (5). In fact, this process can introduce errors for the cases of high sea ice attenuation or thick ice (resulting in a low-valued propagation loss term), in which R_1 and $R_2 e^{-2ik_{zi}d}$ are comparable. In such cases, an interference between the signal components from two interfaces can be expected, and the power of overall echo should be properly evaluated. The absolute SIT difference between the TDS-1 and SMOS results (that are calculated as |SMOS SIT - TDS-1 SIT|/ SMOS SIT) was found to be noticeable with low values (below 0.2) of loss term in sea ice, as presented in Fig. 15. This demonstrates the limitation of the proposed model when attenuation in the ice layer is high and the contribution of R_1 is significant.

Third, according to (10), SIT is dependent on Γ, and therefore, the accuracy of Γ is critical. The estimation of Γ may be affected by the following factors.

1) Transmitted Signal Estimation: Although efforts have been made to approximate the actual transmitted signal by using (2), a constant value of G_d was employed here. This simplification may have caused errors.

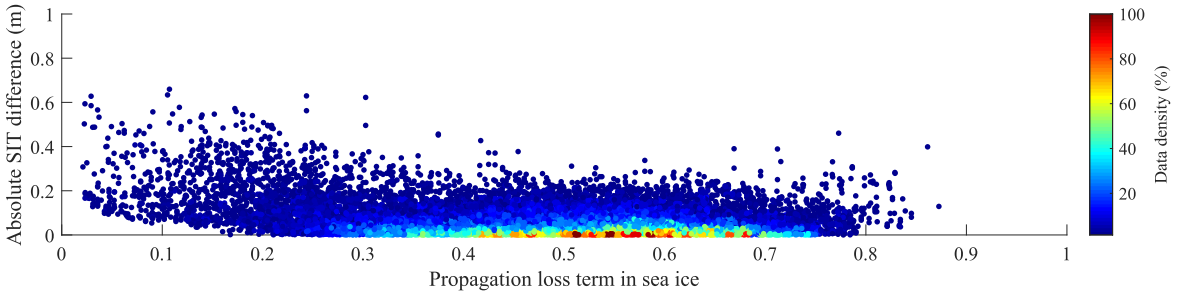

Fig. 15. Impact of the value for loss term on the accuracy of the proposed model. Loss terms with low values (especially below 0.2) introduced noticeable differences. In the case of highly attenuating sea ice, the performance of the proposed model drops.

2) Receiver Antenna Gain: The uncertainty of TDS-1 altitude and orbit was noted in, e.g., [10], which consequently resulted in the uncertainty in G_r.

3) Atmospheric Effects: As shown in [39], such effects may introduce variations in P_r; however, they were neglected in this article.

The error for G_d can be up to 0.8 dB [24]. The median values of the errors in G_r are found to be 0.7 dB through processing TDS-1 data. By only considering such error in the antenna gains, the uncertainty of SIT retrieval can be up to about 30%.

V. Conclusion

In this article, a model for SIT estimation from TechDemoSat-1 GNSS-R data is presented. Here, the reflectivity Γ is constructed as a function of the propagation loss in the sea ice layer and the reflection coefficient of the underneath seawater. By comparing the TDS-1 SIT with the reference data, good consistency is obtained with an r of 0.84 and an RMSD of 9.39 cm for SMOS and an r of 0.67 and an RMSD of 9.49 cm for SMOS/SMAP. Furthermore, another aspect of this method for improving sea ice detection is studied, by comparing Γ with local reflection coefficient.

Although the results obtained show the applicability of the proposed method, the performance of this method for sea ice thicker than 1 m is not examined due to a lack of reliable SIT reference data. Further validation of this method for thick sea ice should be conducted when accurate SIT reference data are available. In addition, as the SMOS/SMAP SIT estimation is also derived with the *L*-band microwave signal and based on similar methodology (propagation attenuation of sea ice), so they can be expected to be correlated with the GNSS-R SIT measurements. It is worth comparing the GNSS-R results with measurements from other sources, such as CryoSat-2 and airborne SIT data once more appropriate data are available. Moreover, when the attenuation in sea ice is significant the proposed model produces noticeable errors. This can be corrected in the future by considering a more comprehensive model. It should be mentioned that the data containing incoherent components due to incoherent reflection from sea-ice covered area are not considered in this article. However, their effect on SIT estimation accuracy should be studied later. It also should be noted that the input of sea ice temperature and salinity are from SMOS data the accuracy of which is unknown and this may be responsible, to some degree, for errors. The accuracy of SIT estimation using GNSS-R can be enhanced in the future when GNSS-R instruments can provide better data or when the effect of error sources (described in Section IV-E) can be mitigated. Furthermore, although an empirical geophysical model function (GMF) method needs a calibration procedure, which is not required in the proposed method, it is worth investigating SIT estimation using an empirical GMF method in the future. More importantly, an enhanced SIT estimation scheme that does not rely on S and T from other sources should be developed in the future so that GNSS-R can produce SIT data independently.

Acknowledgment

The authors would like to thank the TDS-1 team for making their GNSS-R DDM data available at www.merrbys.co.uk.

References

[1] Q. Yan and W. Huang, "Spaceborne GNSS-R sea ice detection using delay-Doppler maps: First results from the U.K. TechDemoSat-1 mission," *IEEE J. Sel. Topics Appl. Earth Observ. Remote Sens.*, vol. 9, no. 10, pp. 4795–4801, Oct. 2016.

[2] A. Alonso-Arroyo, V. U. Zavorotny, and A. Camps, "Sea ice detection using U.K. TDS-1 GNSS-R data," *IEEE Trans. Geosci. Remote Sens.*, vol. 55, no. 9, pp. 4989–5001, Sep. 2017.

[3] D. Schiavulli, F. Frappart, G. Ramillien, J. Darrozes, F. Nunziata, and M. Migliaccio, "Observing sea/ice transition using radar images generated from TechDemoSat-1 delay Doppler maps," *IEEE Geosci. Remote Sens. Lett.*, vol. 14, no. 5, pp. 734–738, May 2017.

[4] Q. Yan and W. Huang, "Detecting sea ice from TechDemoSat-1 data using support vector machines with feature selection," *IEEE J. Sel. Topics Appl. Earth Observ. Remote Sens.*, vol. 12, no. 5, pp. 1409–1416, May 2019.

[5] J. Cartwright, C. J. Banks, and M. Srokosz, "Sea ice detection using GNSS-R data from TechDemoSat-1," *J. Geophys. Res. Ocean.*, Jul. 2019, Art. no. 2019JC015327.

[6] N. Rodriguez-Alvarez, B. Holt, S. Jaruwatanadilok, E. Podest, and K. C. Cavanaugh, "An Arctic sea ice multi-step classification based on GNSS-R data from the TDS-1 mission," *Remote Sens. Environ.*, vol. 230, Sep. 2019, Art. no. 111202.

[7] Q. Yan, W. Huang, and C. Moloney, "Neural networks based sea ice detection and concentration retrieval from GNSS-R delay-Doppler maps," *IEEE J. Sel. Topics Appl. Earth Observ. Remote Sens.*, vol. 10, no. 8, pp. 3789–3798, Aug. 2017.

[8] Q. Yan and W. Huang, "Sea ice sensing from GNSS-R data using convolutional neural networks," *IEEE Geosci. Remote Sens. Lett.*, vol. 15, no. 10, pp. 1510–1514, Oct. 2018.

[9] A. Rius *et al.*, "Feasibility of GNSS-R ice sheet altimetry in greenland using TDS-1," *Remote Sens.*, vol. 9, no. 7, Jul. 2017, Art. no. 742.

[10] J. Cartwright, M. P. Clarizia, P. Cipollini, C. Banks, and M. Srokosz,"Independent dem of antArctica using GNSS-R data from TechDemoSat-1," *Geophys. Res. Lett.*, vol. 45, no. 12, pp. 6117–6123, Jun. 2018.

[11] C. Hu, C. Benson, C. Rizos, and L. Qiao, "Single-pass sub-meter space-based GNSS-R ice altimetry: Results from TDS-1," *IEEE J. Sel. Topics Appl. Earth Observ. Remote Sens.*, vol. 10, no. 8, pp. 3782–3788, Aug. 2017.
[12] W. Li, E. Cardellach, F. Fabra, A. Rius, S. Ribó, and M. Martín-Neira, "First spaceborne phase altimetry over sea ice using TechDemoSat-1 GNSS-R signals," *Geophys. Res. Lett.*, vol. 44, no. 16, pp. 8369–8376, Aug. 2017.
[13] Q. Yan and W. Huang, "Sea ice remote sensing using GNSS-R: A review," *Remote Sens.*, vol. 11, no. 21, Nov. 2019, Art. no. 2565.
[14] S. W. Laxon, N. Peacock, and D. Smith, "High interannual variability of sea ice thickness in the Arctic region," *Nature*, vol. 425, no. 6961, pp. 947–950, Oct. 2003.
[15] K. A. Giles, S. W. Laxon, and A. L. Ridout, "Circumpolar thinning of Arctic sea ice following the 2007 record ice extent minimum," *Geophys. Res. Lett.*, vol. 35, no. 22, Nov. 2008, Art. no. L22502.
[16] S. W. Laxon *et al.*, "CryoSat-2 estimates of Arctic sea ice thickness and volume," *Geophys. Res. Lett.*, vol. 40, no. 4, pp. 732–737, Feb. 2013.
[17] X. Tian-Kunze, L. Kaleschke, and N. Maass, "SMOS daily sea ice thickness version 3," Univ. Hamburg, Germany, 2016.
[18] M. Huntemann, G. Heygster, L. Kaleschke, T. Krumpen, M. Mäkynen, and M. Drusch, "Empirical sea ice thickness retrieval during the freeze-up period from SMOS high incident angle observations," *Cryosph.*, vol. 8, no. 2, pp. 439–451, Mar. 2014.
[19] L. Kaleschke, N. Maaß, C. Haas, S. Hendricks, G. Heygster, and R. T. Tonboe, "A sea-ice thickness retrieval model for 1.4 GHz radiometry and application to airborne measurements over low salinity sea-ice," *Cryosphere*, vol. 4, no. 4, pp. 583–592, Dec. 2010.
[20] D. Mayers and C. Ruf, "Measuring ice thickness with CYGNSS altimetry," in *Proc. IEEE Int. Geosci. Remote Sens. Symp.*, Jul. 2018, pp. 8535–8538.
[21] H. Carreno-Luengo, G. Luzi, and M. Crosetto, "Sensitivity of CYGNSS bistatic reflectivity and SMAP microwave radiometry brightness temperature to geophysical parameters over land surfaces," *IEEE J. Sel. Topics Appl. Earth Observ. Remote Sens.*, vol. 12, no. 1, pp. 107–122, Jan. 2019.
[22] H. Carreno-Luengo, G. Luzi, and M. Crosetto, "Impact of the elevation angle on CYGNSS GNSS-R bistatic reflectivity as a function of effective surface roughness over land surfaces," *Remote Sens.*, vol. 10, no. 11, Nov. 2018, Art. no. 1749.
[23] G. A. Hajj and C. Zuffada, "Theoretical description of a bistatic system for ocean altimetry using the GPS signal," *Radio Sci.*, vol. 38, no. 5, Oct. 2003, Art. no. 1089.
[24] P. Jales and M. Unwin, "Mission description GNSS reflectometry on TDS-1 with the SGR-ReSI," Surrey Satellite Technology Limited, Surrey, U.K., Tech. Rep. 248367, 2015.
[25] S. Gleason, "Space-based GNSS scatterometry: Ocean wind sensing using an empirically calibrated model," *IEEE Trans. Geosci. Remote Sens.*, vol. 51, no. 9, pp. 4853–4863, Sep. 2013.
[26] V. U. Zavorotny, S. Gleason, E. Cardellach, and A. Camps, "Tutorial on remote sensing using GNSS bistatic radar of opportunity," *IEEE Geosci. Remote Sens. Mag.*, vol. 2, no. 4, pp. 8–45, Dec. 2014.
[27] L. Tsang and R. W. Newton, "Microwave emissions from soils with rough surfaces," *J. Geophys. Res.*, vol. 87, no. C11, pp. 9017–9024, Oct. 1982.
[28] F. T. Ulaby, R. K. Moore, and A. K. Fung, *Microwave Remote Sensing: Active and Passive*, vol. 1. Boston, MA, USA: Addison-Wesley, Advanced Book Program/World Science Division, 1982.
[29] R. M. Morey, "Airborne sea ice thickness profiling using an impulse radar," Department of Transportation, United States Coastal Guard, Washington, DC, USA, Tech. Rep. CG-D-178–75, 1975.
[30] D. K. Atwood, G. E. Gunn, C. Roussi, J. Wu, C. Duguay, and K. Sarabandi, "Microwave backscatter from Arctic lake ice and polarimetric implications," *IEEE Trans. Geosci. Remote Sens.*, vol. 53, no. 11, pp. 5972–5982, Nov. 2015.
[31] M. R. Vant, R. O. Ramseier, and V. Makios, "The complex-dielectric constant of sea ice at frequencies in the range 0.1–40 GHz," *J. Appl. Phys.*, vol. 49, no. 3, pp. 1264–1280, Mar. 1978.
[32] F. T. Ulaby, R. K. Moore, and A. K. Fung, *Microwave Remote Sensing: Active and Passive*, vol. 2. Boston, MA, USA: Addison-Wesley, Advanced Book Program/World Science Division, 1986.
[33] V. Zavorotny and A. Voronovich, "Scattering of GPS signals from the ocean with wind remote sensing application," *IEEE Trans. Geosci. Remote Sens.*, vol. 38, no. 2, pp. 951–964, Mar. 2000.
[34] L. Klein and C. Swift, "An improved model for the dielectric constant of sea water at microwave frequencies," *IEEE Trans. Antennas Propag.*, vol. 25, no. 1, pp. 104–111, Jan. 1977.
[35] P. Jales, "Merrbys product manual–GNSS reflectometry on TDS-1 with the SGR-ReSI," Tech. Rep. 248366, 2017.
[36] A. G. Voronovich and V. U. Zavorotny, "Bistatic radar equation for signals of opportunity revisited," *IEEE Trans. Geosci. Remote Sens.*, vol. 56, no. 4, pp. 1959–1968, Apr. 2018.
[37] D. J. Cavalieri, C. L. Parkinson, P. Gloersen and H. J. Zwally, "Sea ice concentrations from Nimbus-7 SMMR and DMSP SSM/I-SSMIS Passive Microwave Data," Boulder, CO: Nat. Snow Ice Data Center, 1996.
[38] D. P. Dee *et al.*, "The era-interim reanalysis: Configuration and performance of the data assimilation system," *Quart. J. Roy. Meteorological Soc.*, vol. 137, no. 656, pp. 553–597, 2011.
[39] G. Foti *et al.*, "Spaceborne GNSS reflectometry for ocean winds: First results from the UK TechDemoSat-1 mission," *Geophys. Res. Lett.*, vol. 42, no. 13, pp. 5435–5441, Jul. 2015.

Qingyun Yan (Student Member, IEEE) was born in Haimen, China. He received the B.Eng. degree in electronic science and engineering from the Nanjing University of Posts and Telecommunications, Nanjing, China, in 2014, and the M.Eng. degree in electrical engineering in 2015 from the Memorial University of Newfoundland, St. John's, NL, Canada, where he is currently working toward the Ph.D. degree in electrical engineering.

His research interests include tsunami detection and sea ice remote sensing using Global Navigation Satellite System-Reflectometry.

Mr. Yan was a recipient of the 2019 IEEE GRSS Letters Prize Paper Award from the IEEE Geoscience and Remote Sensing Society

Weimin Huang (Senior Member, IEEE) received the B.S., M.S., and Ph.D. degrees in radio physics from Wuhan University, Wuhan, China, in 1995, 1997, and 2001, respectively, and the M.Eng. degree in engineering electromagnetics from the Memorial University of Newfoundland, St. John's, NL, Canada, in 2004.

He received the Postdoctoral Fellowship from Memorial University of Newfoundland. From 2008 to 2010, he was a Design Engineer with Rutter Technologies, St. John's. Since 2010, he has been with the Faculty of Engineering and Applied Science, Memorial University of Newfoundland, where he is currently a Professor. He has authored more than 230 research articles. His research interests include the mapping of oceanic surface parameters via high-frequency ground wave radar, *X*-band marine radar, and global navigation satellite systems.

Dr. Huang has been a Technical Program Committee Member. He received the Discovery Accelerator Supplements Award from the Natural Sciences and Engineering Research Council of Canada in 2017. He was a recipient of the IEEE Geoscience and Remote Sensing Society 2019 Letters Prize Paper Award. He served as the Technical Program Co-Chair for the IEEE Newfoundland Electrical and Computer Engineering Conference in 2012 and 2013. He is currently an Associate Editor of IEEE ACCESS and the IEEE CANADIAN JOURNAL OF ELECTRICAL AND COMPUTER ENGINEERING and an Editorial Board Member of *Remote Sensing*. He was a regular Reviewer for over 50 international journals and a Reviewer for many IEEE International Conferences, such as RadarCon, International Conference on Communications, GLOBECOM, IGARSS, and Oceans.